



# Numerical study of fire spread using the level-set method with large eddy simulation incorporating detailed chemical kinetics gas-phase combustion model

T.B.Y. Chen<sup>a</sup>, A.C.Y. Yuen<sup>a,\*</sup>, G.H. Yeoh<sup>a,b</sup>, V. Timchenko<sup>a</sup>, S.C.P. Cheung<sup>c</sup>, Q.N. Chan<sup>a</sup>, W. Yang<sup>d</sup>, H. Lu<sup>d</sup>

<sup>a</sup> School of Mechanical and Manufacturing Engineering, University of New South Wales, Sydney, NSW 2052, Australia

<sup>b</sup> Australian Nuclear Science and Technology Organisation (ANSTO), Locked Bag 2001, Kirrawee DC, NSW 2232, Australia

<sup>c</sup> School of Aerospace, Mechanical and Manufacturing Engineering, RMIT University, Victoria 3083, Australia

<sup>d</sup> Department of Chemical and Materials Engineering, Hefei University, Hefei, Anhui 230601, People's Republic of China



## ARTICLE INFO

### Article history:

Received 11 April 2017

Received in revised form 18 October 2017

Accepted 18 October 2017

Available online 21 November 2017

### Keywords:

Wildland fire

Level-set method

Detailed chemistry

Large Eddy Simulation

Combustion modelling

## ABSTRACT

A fire code has been developed for the purpose of modelling wildland fires via Large Eddy Simulation (LES) and the use of the level-set approach to track the flame front. Detailed chemical kinetics have been considered via the strained laminar flamelet approach for the combustion process which included the consideration of the yields of toxic volatiles such as CO, CO<sub>2</sub> and soot production. Numerical simulations have been validated against an experimental study on the fire spread on a pine needle board under different slope angles. Peak temperatures and occurrence times during the propagation process were predicted with an overall average error of 11% and 3% respectively. This demonstrates that the flaming behaviour could be well predicted under different slope conditions. By incorporating the level set with the gas phase models, information including temperature field, toxic volatiles and soot particle concentrations can be realised in comparison to empirical fire spread models.

© 2017 Elsevier B.V. All rights reserved.

## 1. Introduction

Bushfires are frequently occurring fire incidents that could significantly disrupt the natural habitat and ecological system as well as affect prime agricultural land for animal grazing and dairy production. In Australia alone, the landscape comprises of a majority of grasslands that are frequently ravaged by bushfires due to the prevailing hot and dry climate. One renowned fire incident was the occurrence of the Black Saturday bushfires which took place in the state of Victoria on February 2009. This fire incident claimed 173 lives, 413 injuries and an estimated total loss of 4.5 billion Australian dollars [1]. Good knowledge and understanding of the coupled physical and chemical behaviours involved during bushfires is essential for the prevention, planning and response, as well as recovery during such outbreaks which can reduce the massive damage to vegetation as well as human fatalities. Furthermore, the knowledge can also result in better planning and design of suburban areas and towns for fire hazard reduction and safety.

Understanding bushfires (also known as wildland fires) generally involve the utilisation of modern numerical methods to predict the fire spread behaviours. Fire spread models have been employed to assist analysts and firefighters to assess a multitude of situations and deploy different suppression strategies. In general, the fire spread models of wildland fires can be categorised into two broad approaches [2]: (i) physical models that attempt to represent the fundamental heat transfer and combustion mechanics; and (ii) empirical or semi-empirical models that are correlated by physical data obtained through laboratory experiments and real life bushfire incidents. In the past, fire spread models primarily aimed to investigate the rate of spread (ROS) and the involving burning region [3]. A typical empirical correlated fire spread models require the following variables as input to evaluate ROS: (i) the characteristics and quantification of the fuel (i.e. the total fuel load, moisture content and the combustion characteristics of the fuel); (ii) atmospheric conditions (i.e. wind speed, wind direction, temperature and humidity of surrounding air); (iii) topology of the landscape (i.e. surface area, ignition point and slope angle); (iv) and lastly, the characteristics of the fire (i.e. flame intensity and height).

The empirical model of Rothermel [4] has been extensively used in the wildland fire spread community within the United States of

\* Corresponding author.

E-mail address: [c.yuen@unsw.edu.au](mailto:c.yuen@unsw.edu.au) (A.C.Y. Yuen).

America [5]. It has formed the foundation for the development of many fire prediction systems. For example, the National Fire Danger Rating System [6] and BEHAVE [7] Fire Prediction System. This model was developed based on the combination of wind tunnel experiments on fuel beds [8] and field experiments of grassfires in Australia [9]. Rothermel's model had also gained a level of utilisation in several countries outside of the United States, such as Europe [10]. Currently, the fire spread model of Rothermel remains the core fire behaviour model in the US but support for other alternatives such as Balbi et al. [11] is actively growing in the community. The Canadian Fire Behaviour Prediction (FBP) System was a fire spread model that was parameterised for Canadian vegetation and climate developed by The Forestry Canada Fire Danger Group [12]. It is implemented in the Canadian Forest Fire Danger Rating System (CFFDRS) as well as the New Zealand Fire Danger Rating System. A detailed review of other empirical and quasi-empirical fire spread models can be found in Sullivan [3]. Although it is always ideal to use real life data to validate the fire spread models, it is difficult to apply them in a wider scope of applications since they are mostly based on specific experimental configurations. Furthermore, the performance of empirical fire models relies heavily on the quality of the input parameters and providing accurate inputs into the model can be very difficult to achieve in reality. Different techniques have been developed to minimise the uncertainty in model inputs and improve the efficiency of these models. For example, Bianchini et al. [13] developed an Evolutionary-Statistical System (ESS) that attempt to adjust input parameters in real time. Sanjuan et al. [14] developed a map partitioning method to minimise wind field uncertainty for fire spread prediction.

Application of mathematical modelling on bushfires has become increasingly popular due to the rapid advancement of numerical methodologies and computational power. These range from basic flame front tracking models such as FARSITE [15], BehavePlus [7] and PHOENIX-rapidfire [16] and many others [17,18] to complex three-dimensional (3D) computations fluid dynamics (CFD) models such as FIRETEC [19] and WFDS [20]. Flame front tracking models simulate the spread of fire without implementing the pyrolysis process of grasslands or vegetation. These are so-called front tracking tools that consist of various algorithms designed to expand a fire perimeter base on a set of rules that govern the rate of fire spread. The spread rate is often calculated from empirical models. Therefore, they can also be described as extensions of empirical models to take advantage of the rapid advancements in numerical methods and computational power. The front tracking approach is also compatible on a regional scale perspective (i.e. tens to hundreds of kilometres). The flame front is represented as a two-dimensional interface thus, giving a considerable saving in computational cost over three-dimensional CFD models. The two most common methods used in this type of fire propagation are the cellular method and level-set method. Both approaches discretise the surface into a grid. Cellular methods update the state of the grid over time according to a rule set that assumes the shape of the fire front such as an elliptical shape [21].

Level-set method [22] is a more recent approach that does not require any prior assumptions on the shape of the fire front. In this method, the fire front is described as a discretised set of cells that expand at a given rate of spread. The state of each cell is represented by the value of the level-set function. This approach offers a few key advantages for modelling wildland fire spread. The calculation of the fire spread rate is highly dependent on the fuel properties and environmental conditions that can vary across the landscape. These variables can be stored at each individual cell to compute a variable spread rate that evolves according to the vegetation and topology. In addition, the level-set method is able to calculate the normal vector to the fire front which is also necessary to model wind-aided fire spreads. The merging of separate fire fronts is handled

automatically without any additional algorithm and the ignition points naturally evolved into an elliptical form, according to the test conducted by Rehm and McDermott [23]. Moreover, the level-set method is relatively easy to implement and couple with physical based models because the same computational grid can be used by both models. In summary, the level-set is a very powerful method to track the propagation of wildland fire spread and have been incorporated by many fire models such as BEHAVE [7] and WRF-SFIRE [24].

Currently, physical fire spread models of wildland fires adopt a single- or two-step simplified chemistry combustion model. FIRETEC [19] is a three-dimensional wildland fire model that uses a hydrodynamics model HIGRAD [25,26] specifically to solve high gradient atmospheric flows. FIRETEC incorporates a simplified single-step solid-gas phase reaction to model the entire combustion process. A critical temperature of 500 K [19] is used as an ignition criteria for combustion (i.e. the combustion process is initialised when the temperature exceeds 500 K). The Wildland Fire Dynamic Simulator (WFDS) is built upon the widely recognised Fire Dynamic Simulator (FDS), designed to simulate fires within building compartments [27]. It is developed by the National Institute of Standards and Technology (NIST) and the US Forest Services. WFDS incorporates a multiphase fire propagation model by Morvan and Dupuy [28]. The model operates under the assumption that combustion occurs predominantly above the surface fuel bed. It incorporates solid fuel pyrolysis which is assumed to occur at a temperature of 127 °C. Gas phase combustion is modelled with a mixture fraction based approach using a single-step reaction. Thermal Radiation is simulated using the P1 radiation model and soot production is assumed as a fraction of the mass of fuel gas consumed during combustion [29]. A sub-grid scale (SGS) turbulence based on Large Eddy Simulation (LES) is used to describe the turbulence flow [30]. The consideration of detailed chemistry combustion is a relatively new area in the field of wildland fire modelling. This is mainly due to the fact that detailed chemistry combustion models are usually not practical owing to its enormous amount of computational burden, which is attribute to the numerous chemical reactions and species needed to be considered and resolved, as well as the demand of a highly refined computational grid size (<1 m) [31]. Thus far a trade-off to simplify the comprehensive kinetic schemes while maintaining prediction accuracy remains a challenge [32].

On the other hand, the majority of empirical fire spread models underestimate the effect of slope on the rate of fire spread. In recent years, a considerable amount of efforts have been made to address the heat transfer mechanisms and the influence of slope on the rate of fire spread [33–35]. However, these models remain unsuccessful for higher slope angles (especially for angles greater than 20°) [36]. Although the two main approaches (physical and empirical) to fire modelling are mainly developed to serve different purposes, coupling the two into a hybrid model could have potential to overcome the limitations of existing fire spread models. In this study, a fire code has been developed for the purpose of modelling wildland fires via Large Eddy Simulation (LES) and the use of the level-set approach to track the flame front. The aim is to provide additional information on the flaming behaviours which cannot be produced by empirical fire spread models. This includes the prediction of combustion rate, intermediate and major gas species, as well as smoke production. Furthermore, this study will provide a preliminary study to investigate the viability of coupling the level-set method with detailed chemistry combustion and create the framework for a fully coupled fire spread model with two-way interaction between the fire spread model and combustion model. The key objectives can be summarised in the following:

**Table 1**

Input variables for Rothermel's fire spread model.

Input	Description
$w_0$	Ovendry fuel load ( $\text{lb ft}^{-2}$ )
$\delta$	Fuel depth (ft)
$\sigma$	Surface area to volume ratio ( $\text{ft}^{-1}$ )
$h$	Heat content ( $\text{Btu lb}^{-1}$ )
$\rho_p$	Ovendry particle density ( $\text{lb ft}^{-3}$ )
$M_f$	Fuel moisture content (%)
$S_T$	Fuel mineral content (%)
$S_e$	Fuel effective mineral content (%)
$U$	Wind ( $\text{ft min}^{-1}$ )
$M_x$	Moisture content of extinction (%)
$\tan \theta$	slope

- a fire code incorporating the fire spread model coupled with detailed chemical kinetics will be developed;
- numerical simulations will be performed using the developed fire code on flame spread experimental studies;
- with the consideration of detailed chemical kinetics, the proposed model will be able to provide a complete description of the generation of asphyxiant gas such as Carbon Monoxide (CO), Carbon Dioxide ( $\text{CO}_2$ );
- the formation of soot particles will be approximated by a semi-empirical soot formation model based on the concentration of acetylene ( $\text{C}_2\text{H}_2$ ), which will provide a brief estimation of the smoke layer formed at the flame front; and
- the inclusion of all essential predictions for soot formation and gaseous products, the radiation heat transfer at the flame front and its corresponding hot fire plume that could be properly modelled in a bushfire scenario.

## 2. Computation code

An in-house fire code has been proposed through the use of the Large Eddy Simulation (LES) framework, a level-set based fire spread model, gas phase combustion model associated with detailed chemical kinetics, subgrid-scale (SGS) turbulence, soot formation and radiation models. As indicated in Fig. 1, the fire spread model implemented in this study utilises a semi-empirical spread rate model proposed by Rothermel [4]. The fire spread rate model can be altered to account for different fuel types or geographical applicability. The level-set methodology is adopted to track the flame front based on the resolved fire spread rate, which will be described in the following section.

### 2.1. Fire spread rate

The fire spread rate is calculated using Rothermel's [4] mathematical model. This model is well documented in literature; it relates the fire spread rate to wind and slope angle where both effects are combined additively. The fire spread rate  $R_s$  is calculated by the general formula:

$$R_s = R_0 (1 + \phi_w + \phi_s) \quad (1)$$

where  $R_0$  is the spread rate without wind and slope,  $\phi_w$  and  $\phi_s$  are the wind and slope coefficients respectively. The coefficients are functions of a variety of other input variables listed in Table 1. Detailed formulation of each coefficient are summarised and tabulated in Table 2. The model inputs were originally developed for imperial units, and therefore the model inputs were converted to empirical units for the calculations and the results (i.e. the fire spread rate) were then converted back from the original  $\text{ft. min}^{-1}$  to  $\text{m s}^{-1}$ .

**Table 2**

Formulation for Rothermel's fire spread model.

$R_0 = \frac{I_R \xi}{\rho_b \varepsilon Q_{ig}}$	Spread rate without wind
$I_R = \Gamma' w_n h \eta_M \eta_S$	Reaction intensity
$\Gamma' = \Gamma'_{\max} (\beta/\beta_{op})^A \exp[A(1 - \beta/\beta_{op})]$	Optimum reaction velocity
$\Gamma'_{\max} = \sigma^{1.5} (495 + 0.0594\sigma^{1.5})^{-1}$	Maximum reaction velocity
$\beta_{op} = 3.348\sigma^{-0.8189}$	Optimum packing ratio
$A = 1/(4.774\sigma^{0.1} - 7.27)$	
$\eta_M = 1 - 2.59 \frac{M_f}{M_x} + 5.11 \left( \frac{M_f}{M_x} \right)^2 - 3.52 \left( \frac{M_f}{M_x} \right)^3$	Moisture damping coefficient
$\eta_S = 0.174 S_e^{-0.19}$	Mineral damping coefficient
$\xi = (192 + 0.2595\sigma)^{-1} \exp[(0.792 + 0.681\sigma^{0.5})(\beta + 0.1)]$	Propagating flux ratio
$\phi_w = C U^B \left( \frac{\beta}{\beta_{op}} \right)^{-E}$	<b>Wind coefficient</b>
$C = 7.47 \exp(-0.133\sigma^{0.55})$	
$B = 0.02526\sigma^{0.54}$	
$E = 0.715 \exp(-3.59 \times 10^{-4}\sigma)$	
$w_n = \frac{w_0}{1 + S_T}$	Net fuel loading
$\phi_S = 5.275 \beta^{-0.3} (\tan \phi)^2$	<b>Slope factor</b>
$\rho_b = w_0/8$	Ovendry bulk density
$\varepsilon = \exp(-138/\sigma)$	Effective heating number
$Q_g = 250 + 1116 M_f$	Heat of preignition
$\beta = \frac{\rho_b}{\rho_p}$	Packing ratio

**Table 3**

Definition of level set function values.

Level set Function	State
$\varphi(x, t) \leq 0$	Burning region
$\varphi(x, t) = 0$	Fire front
$\varphi(x, t) > 0$	No Fire

### 2.2. Fire spread model

The fire spread model used in this study incorporates the level-set method [37] to simulate the propagation of the flame front. The level-set method is a form of flame front tracking where the fire perimeter is described as a discretised set of cells that expand according to a given rate of spread  $R_s$ . The fire spread model was implemented on block surfaces on the x-y plane facing towards the +ve z-direction to replicate the fire spread along the pine needles board of the numerical case study which will be illustrated in the upcoming section, in which x and y are the horizontal and the span-wise or lateral direction respectively while z depicts the vertical height. Each grid cell maintained a level-set function  $\varphi$ , and a spread rate  $R_s$ , calculated by Rothermel's [4] formulation using the fuel characteristics and slope angle that are specific to the blocks and a global wind speed. In this model, the level-set term  $\varphi(x, t)$  governs the fire condition, which can be represented by Table 3.

The level-set function  $\varphi$  is determined by the equation devised by Osher and Fedkiw [38]:

$$\frac{\partial \varphi}{\partial t} + R_s |\nabla \varphi| = 0 \quad (2)$$

where  $R_s = n \cdot \partial x / \partial t$  represent the fire spread rate in the direction  $n$ , defined as the unit normal vector  $\nabla \varphi / |\nabla \varphi|$  calculated using central differencing. The level-set function solution is advanced in time by the following equations:

$$\varphi^{n+1/2} = \varphi^n + \Delta t F(\varphi^n) \quad (3)$$

$$\varphi^{n+1} = \varphi^n + \Delta t \left( \frac{1}{2} F(\varphi^n) + \frac{1}{2} F(\varphi^{n+1/2}) \right) \quad (4)$$

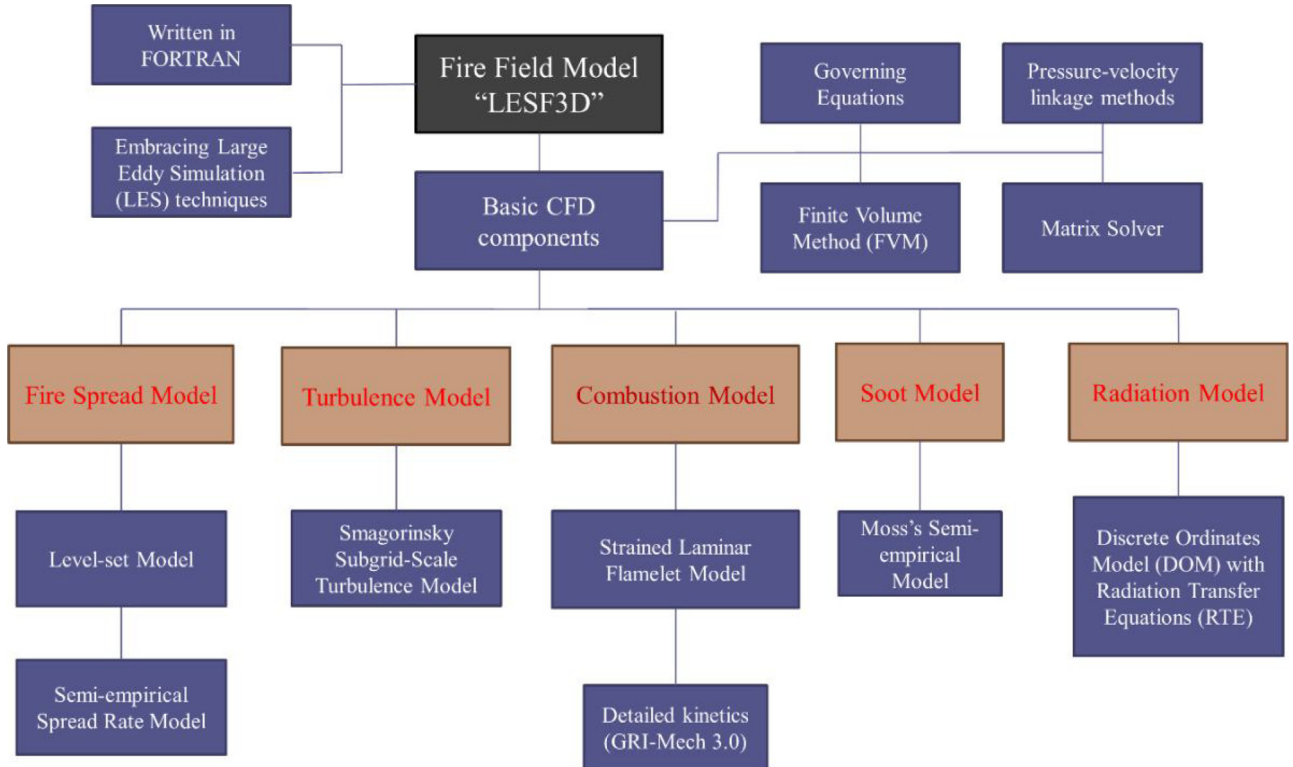


**Fig. 1.** Schematic diagram of the present fire code showing the fire spread model and other essential modelling components.

where  $F(\varphi^n) = R_s |\nabla \varphi|$  denotes the advective term of the level-set equations shown in Eq. (2) and the scalar gradient  $\nabla \varphi$  is approximated using the essentially non-oscillatory (ENO) method:

$$\bar{\nabla}_x \varphi = \begin{cases} \bar{\nabla}_x^+ \varphi & \text{if } \bar{\nabla}_x^- \varphi \leq 0 \quad \text{and} \quad \bar{\nabla}_x^+ \varphi \leq 0 \\ \bar{\nabla}_x^- \varphi & \text{if } \bar{\nabla}_x^- \varphi \geq 0 \quad \text{and} \quad \bar{\nabla}_x^+ \varphi \geq 0 \\ \bar{\nabla}_x \varphi & \text{if } \bar{\nabla}_x^- \varphi \geq 0 \quad \text{and} \quad \bar{\nabla}_x^+ \varphi \leq 0, \quad \text{and} \quad |\bar{\nabla}_x^- \varphi| \geq |\bar{\nabla}_x^+ \varphi| \\ \bar{\nabla}_x^+ \varphi & \text{if } \bar{\nabla}_x^- \varphi \geq 0 \quad \text{and} \quad \bar{\nabla}_x^+ \varphi \leq 0, \quad \text{and} \quad |\bar{\nabla}_x^- \varphi| \leq |\bar{\nabla}_x^+ \varphi| \\ \text{else, } 0 & \end{cases} \quad (5)$$

where  $\bar{\nabla}_x^+ \varphi$  and  $\bar{\nabla}_x^- \varphi$  are the forward and backward differences given by:

$$\bar{\nabla}_x^+ \varphi(x, z) = \frac{\varphi(x + \Delta x, z) - \varphi(x, z)}{\Delta x} \quad (6)$$

$$\bar{\nabla}_x^- \varphi(x, z) = \frac{\varphi(x, z) - \varphi(x - \Delta x, z)}{\Delta x}, \quad (7)$$

The level-set terms are initialised for the discretised block surfaces in this proposed fire spread model by allocating positive unity value (+1) to represent unburned surfaces. In order to initiate a fire, a value of negative unity (-1) is inserted on one of the block surface, which will eventually affect adjacent blocks according to the rate of spread  $R_s$ . The simulations in this study are based on the experiments by Liu et al. [36] to investigate 'linear' flame spread under different slope and no ambient wind conditions. Therefore, with the absence of a wind factor and wind direction, the linear fire front will propagate uniformly across the fuel bed. As illustrated in Fig. 2, provided the spread rate is positive (i.e. the fire is propagating in the  $x$ -direction) and the fire is ignited at the surface  $\varphi_{x,i}$ , the level-set term for the adjacent block surface  $\varphi_{x,i+1}$  will decrease after every iterative time step based on the negativity of the previous term and the magnitude of the spread rate. Once a block surface is considered as the flame front ( $\varphi=0$ ), or burning region ( $\varphi<0$ ), a constant gas-phase fuel injection rate towards the positive  $z$ -direction is applied

at the surface. The fuel injection rate is calculated according to a normalised mass loss rate of pine needle obtained using small-scale calorimetry by Jervis and Rein [39]. Furthermore, each block surface is prescribed with a total fuel load value which governs the remaining amount of fuel. This value decreases according to the mass loss within the block due to fuel injected to the fluid domain. When this value approaches zero which denote fuel is totally consumed, the fuel injection rate will be forced to zero.

### 2.3. Governing equations

In LES, the Favre-filtering approach is applied to the conservation laws governing a Newtonian fluid in the physical space. A generic transport equation can be applied for the mass, momentum, energy, and other scalar properties. The general form can be expressed as:

$$\underbrace{\frac{\partial (\bar{\rho} \psi)}{\partial t}}_{T_\psi} + \underbrace{\frac{\partial (\bar{\rho} \tilde{u}_i \psi)}{\partial x_i}}_{C_\psi} = \underbrace{\frac{\partial}{\partial x_i} \left( \gamma_\psi \frac{\partial \psi}{\partial x_i} \right)}_{D_\psi} + \bar{s}_\psi \quad (8)$$

where  $\psi$  is the field dependent variable,  $T_\psi$  is the unsteady term,  $C_\psi$  is the convection term,  $D_\psi$  is the diffusion term with diffusion coefficient  $\gamma_\psi$  and  $\bar{s}_\psi$  is the source term. The corresponding expressions for the diffusion coefficients and the source terms for field-dependent including velocity, temperature, mixture fraction, variance of mixture fraction, soot mass fraction and particulate number density are tabulated in Table 4. In the diffusion coefficient term,  $\mu$  and  $\mu_T$  are the dynamic and turbulent viscosity respectively.  $Sc$  and  $Pr$  are the Schmidt and Prandtl number respectively, where the subscript  $T$  indicates the turbulent components.  $C_p$  and  $\rho$  are the specific heat capacity and density of the fluid mixture respectively.

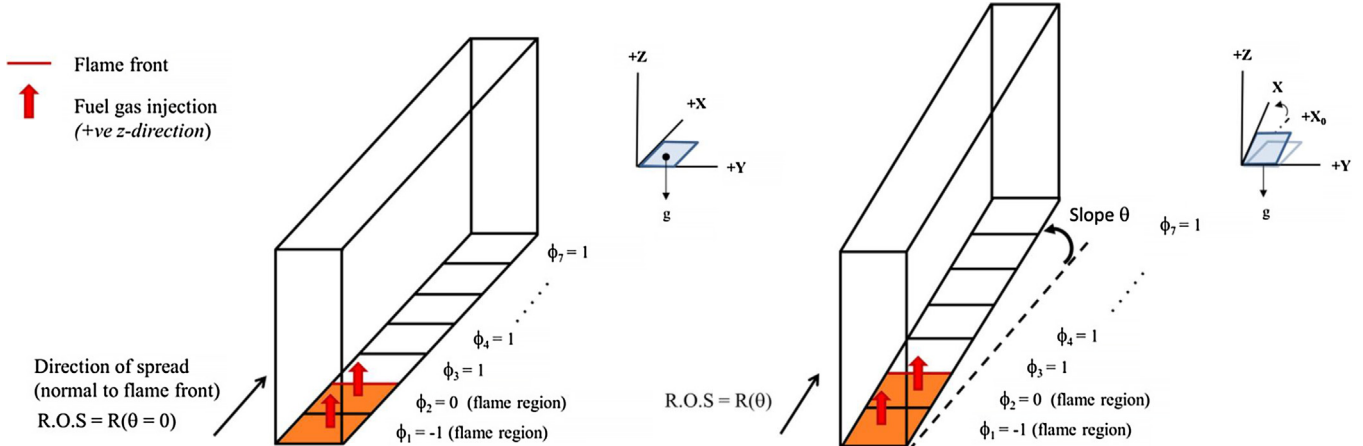


**Fig. 2.** Schematic sketch of the fire spread rate effect on level set term and fuel gas injection.

**Table 4**

Field-dependent variable, diffusion coefficient, and source terms of the generalized transport equation. (velocity  $\tilde{u}$ , temperature  $\tilde{T}$ , mixture fraction  $\zeta$ , variance of mixture fraction  $\zeta'$ , soot mass fraction  $M_{soot}$  and particulate number density  $\eta_{soot}$ ).

field dependent variable $\psi$	diffusion coefficient $\Upsilon_\psi$	source term $S_\psi$
$\tilde{u}_j$	$\mu + \mu_T$	$-\frac{\partial \bar{p}}{\partial x_i} + \frac{\partial}{\partial x_j} \left[ (\mu + \mu_T) \frac{\partial \tilde{u}_j}{\partial x_i} \right] - \frac{\partial}{\partial x_j} \frac{2}{3} (\mu + \mu_T) \frac{\partial \tilde{u}_k}{\partial x_k} \delta_{ij} + \bar{S}_u$
$C_p \tilde{T}$	$\frac{\mu}{P_T} + \frac{\mu_T}{P_{T_T}}$	$S_{\bar{w}_T} + \bar{S}_{rad}$
$\zeta$	$\frac{\mu}{Sc} + \frac{\mu_T}{Sc_T}$	0
$\zeta'$	$\frac{\mu}{Sc} + \frac{\mu_T}{Sc_T}$	$2 \left( \frac{\mu}{Sc} + \frac{\mu_T}{Sc_T} \right) \frac{\partial \tilde{\zeta}}{\partial x_i} \frac{\partial \tilde{\zeta}}{\partial x_j} - \bar{\rho} \bar{\chi}$
$M_{soot}$	$\frac{\mu_T}{Sc_T}$	$S_{M_{soot}}$
$\eta_{soot}$	$\frac{\mu_T}{Sc_T}$	$S_{\eta_{soot}}$

#### 2.4. Combustion modelling

The strained laminar flamelet combustion model is adopted in this study by which the fluctuation, microscopic fuel air mixing and effect of turbulence are accounted for. Two field variables including the mixture fraction and its variance are solved through this model. A new parameter known as the “scalar dissipation” is established to describe the non-uniformity of the flame from its initial chemical equilibrium state, or in other words how much straining the flame is being experienced. By prescribing the beta form of the Probability Density Function (PDF), the influence of the scalar dissipation and time-dependent fluctuations of mixture fraction on the flamelets can be fitted into a generated flamelet “look-up table”, which will be further illustrated in Section 2.3. On the basis of the previous version of the presented in-house fire field model [32], the field mass fraction within the grid control volume for each individual chemical species can be related to the flamelets and PDF as:

$$\tilde{m}_{s_i} = \int_0^1 M_{s_i}(\zeta, \zeta', \chi) P(\zeta, \zeta', \chi) d\zeta \quad (9)$$

where  $M_{s_i}(\zeta, \zeta', \chi)$  is the generated flamelet table for mass fraction in function of mixture fraction  $\zeta$ , variance of mixture fraction  $\zeta'$ , as well as the scalar dissipation rate  $\chi$ . The subscript  $s_i$  denotes the  $i$ -th species in consideration.  $P(\zeta, \zeta', \chi)$  is the corresponding beta PDF function. As proposed by Jiménez et al. [40] a simplified generalised model for the scalar dissipation can be formulated based on Yoshizawa's model [41] and SGS turbulent kinetic energy formula:

$$\chi = \frac{1}{\rho} \frac{(\mu + \mu_T)}{Sc_{T,\zeta'} C' \Delta^2} \zeta' \quad (10)$$

where  $Sc_{T,\zeta'}$  is the turbulent Schmidt number for mixture fraction variance defined as 0.3,  $\Delta$  is the SGS filter length related to the size of the grid control volume evaluated as  $\Delta = \sqrt[3]{\Delta x \Delta y \Delta z}$ , the parameter  $C'$  can be given as 0.07 for accurate predictions of dissipation locally and on average [40]. Finally, the heat release rate source term due to combustion is computed based on the simplified model proposed by Bilger [42]. This expression is generated by relating the source term in the transport equation of the mixture fraction variance to the scalar dissipation:

$$S_{\omega_T} = \frac{1}{2} \rho \chi \sum_{s_i=1}^N \left[ \int_0^1 \left( h_{s_i} \frac{d^2 M_{s_i}}{d\zeta'^2} P(\zeta, \zeta', \chi) \right) d\zeta \right] \quad (11)$$

where the subscript  $\omega_T$  indicates the total heat release rate in the grid control volume,  $h_{s_i}$  depicts the heat of formation for the corresponding  $i$ -th species. In this model, the heat generated by combustion is highly related to second order derivative of the species mass fraction. It should be noted that the peak values for the second deviates usually occurred at the stoichiometric mixture fraction values, meaning the point where the amount of oxygen is exactly sufficient to be totally consumed by the fuel. Therefore, most of the flame will take place at the interface between the flaming region and surrounding air. Since the proposed strain laminar flamelet model requires only the mass fraction and its second derivatives for various species under different flame strain and mixture fraction conditions in a “look-up table” manner, the model is able to handle a vast amount of chemical kinetics and intermediate species without resolving them every iteration steps.

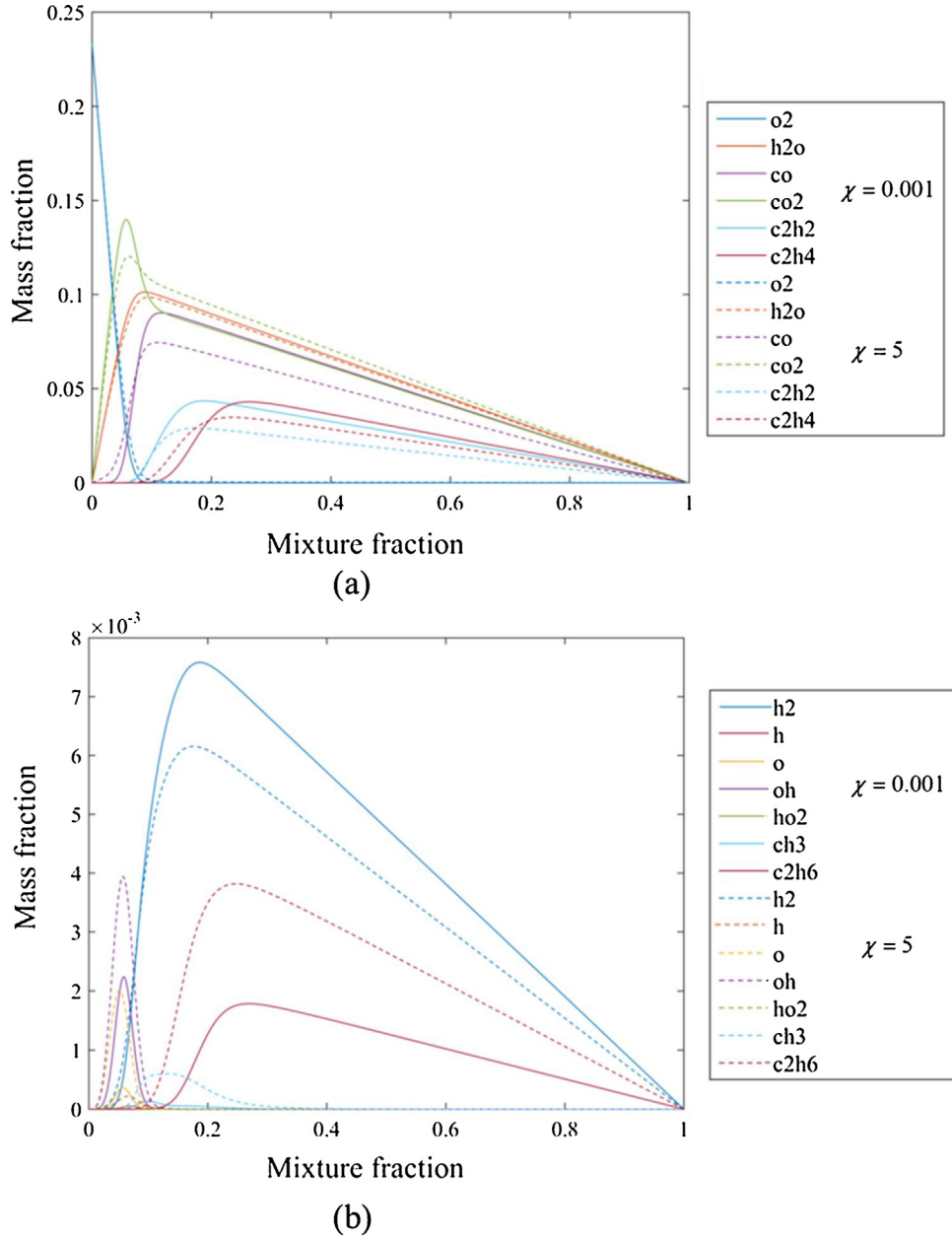


Fig. 3. Flamelet profiles for (a) major and (b) minor species for scalar dissipation rates:  $\chi = 0.001$  and  $\chi = 5$ .

## 2.5. Flamelet library construction

In this study, the parent fuel for the gas-phase combustion is taken as formaldehyde ( $\text{CH}_2\text{O}$ ), which is commonly used as an analogy for the volatile gas resulted in the pyrolysis of wooden materials [43]. Based on numerous experimental work on wood, the gas volatiles has a mean molecule form of  $\text{CH}_2\text{O}$  [44]. The detailed chemical kinetics for the GRI-Mech 3.0 [45] and CHEMKIN 3.6 [46] was utilised to generate the flamelet library in function of mixture fraction and its variance, as well as scalar dissipation rate. The GRI-MECH 3.0 containing 325 reactions and 53 species. The model allows more accurate prediction of the oxidation process of the fuel in comparison to single-step and multi-steps reaction mechanisms, as well as key partial chemical products including  $\text{CO}$ ,  $\text{OH}$ ,  $\text{H}_2$  and  $\text{C}_2\text{H}_2$ . Furthermore,  $\text{C}_2\text{H}_2$  could be considered as the main soot precursor in the semi-empirical soot model, which provides a much better representation of the soot nucleation, surface growth and oxidation processes. A total of 20 flamelet profiles were gen-

erated with distinct scalar dissipation rates  $\chi$  ranging from 0.001 to 76. Fig. 3 (a), (b) shows the flamelet profiles of major and selective minor species at two scalar dissipation rates ( $\chi = 0.001$  and  $\chi = 5$  respectively). It should be noted that the major species were selected based on a mass fraction cut-off of 0.01 (i.e. mass fraction greater than 0.01). During the simulation, chemical species with mass fraction less than  $1.0\text{E-}5$  were not resolved to optimise the computational efficiency of the detailed chemistry CFD code. The amount of  $\text{NO}_x$  production was found to be smaller than the cut-off fraction and also taken into consideration that the case study consists of burning a very thin layer of pine needles under well-ventilated conditions, the  $\text{NO}_x$  emission was not modelled in the simulation. As a result, a total number of 14 species were considered in the simulation.

The theoretical stoichiometric mixture fraction  $\zeta_{st}$  for  $\text{CH}_2\text{O}$  is around 0.179. Incomplete combustion occurs for mixture fractions larger than the stoichiometric value. As shown in Fig. 3 (a), the major combustion products such as  $\text{CO}_2$  and  $\text{H}_2\text{O}$  peak before  $\zeta_{st}$

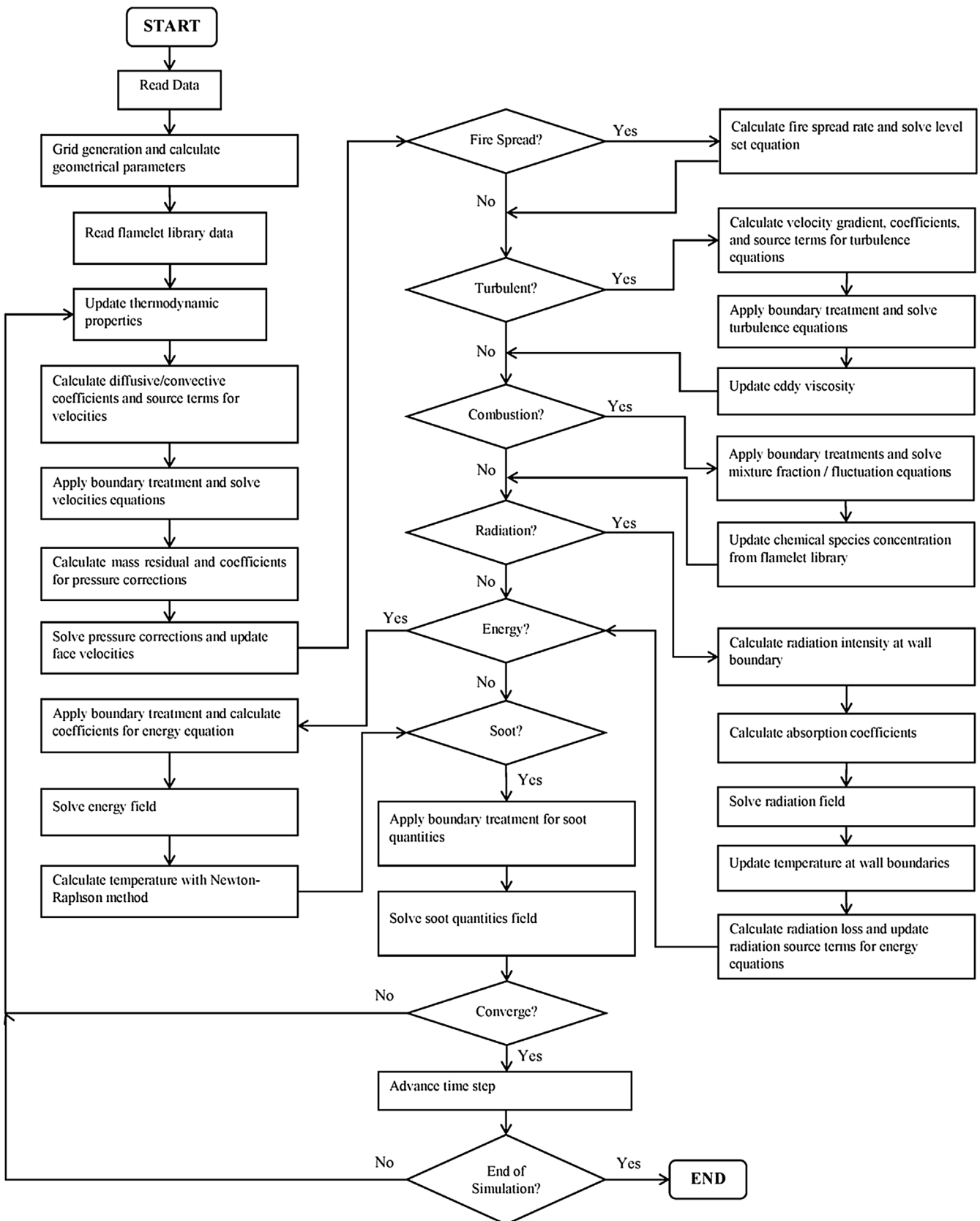


**Fig. 4.** Flow chat diagram showing the logical flow of the present fire code.

while intermediate species such as CO and C<sub>2</sub>H<sub>2</sub> peak after  $\zeta_{st}$ . When the scalar dissipation increases, the flame is suppressed due to the separation of fuel and oxidant and the majority of combustion products decreases as less fuel is burnt. It is found that the flame is close to extinction around  $\chi = 76$ .

## 2.6. Turbulence modelling

The mathematical formulations of the LES adopted in this study is based on the density-weighted Favre filtering of mass, momentum, energy and scalar quantities governing equations with Smagorinsky SGS turbulence [47]. The SGS momentum stress is modelled according to Smagorinsky [48]:

$$\bar{\tau}_{ui} u_j \approx 2\mu_T \left( \tilde{S}_{ij} - \frac{1}{3} \tilde{S}_{kk} \delta_{ij} \right) - \frac{1}{3} \bar{\tau}_{kk} \delta_{ij} \quad (12)$$

And  $\bar{\tau}_{kk} = 2C_l \rho \Delta^2 |(2\tilde{S}_{ij} \tilde{S}_{ij})^{(1/2)}|$ , where  $C_l$  is an empirical constant and the strain rate tensor  $\tilde{S}_{ij} = \frac{1}{2} \left( \frac{\partial \tilde{u}_i}{\partial x_j} + \frac{\partial \tilde{u}_j}{\partial x_i} \right)$ .

The turbulent viscosity  $\mu_T$  is given by

$$\mu_T = \bar{\rho} (C_s \Delta)^2 |(2\tilde{S}_{ij} \tilde{S}_{ij})^{(1/2)}| \quad (13)$$

The Smagorinsky constant  $C_s$  is taken to be a value of 0.2 while the turbulent Prandtl and all the scalar turbulent Schmidt numbers are prescribed at values of 0.30 [48]. Erlebacher et al. [49] suggested that the term  $\bar{\tau}_{kk}$  may be ignored since  $C_s \gg C_l$  and the value is extremely small.

## 2.7. Soot formation modelling

When considering the modelling of soot particles, it is inevitable to account for several key particle generation/reduction processes which include particle inception/nucleation, surface growth, coagulation, agglomeration, as well as oxidation [32,50]. Since the detailed chemical kinetics and the modelling of intermediate chemical species are involved in the combustion model, a more comprehensive description of the kinetics for the soot formation process is enabled. Based on the study of reaction mechanisms on the soot formation for non-premixed combustion flames reported by Leung et al. [51], it is discovered that the particle inception and surface growth of soot particles can be conveniently correlated to the concentration of acetylene (C<sub>2</sub>H<sub>2</sub>). In this study, a two-equation semi-empirical soot model proposed by Brookes and Moss [52] is implemented where acetylene is considered as the soot precursor. In this model, an average value for the number density and mass fraction of soot particles are solved to reflect the amount of soot concentration within the computational field, in which changes are entirely governed by the source terms.

For soot mass fraction, the source term is given by the following expression:

$$SM_{soot} = C_\alpha W_{soot} \left( \frac{Z_{C_2H_2} \tilde{P}}{R_{gas} \tilde{T}} \right) \exp \left( -\frac{E_\alpha}{\tilde{T}} \right) + C_\gamma \left( \frac{Z_{C_2H_2} \tilde{P}}{R_{gas} \tilde{T}} \right)^{2/3} \exp \left( -\frac{E_\gamma}{\tilde{T}} \right) \left[ (\pi \eta_{soot})^{1/3} \left( \frac{6M_{soot}}{\rho_{soot}} \right)^{2/3} \right] - C_\omega C_{coll} \left( \frac{Z_{OH} \tilde{P}}{R_{gas} \tilde{T}} \right) \sqrt{\tilde{T}} (\pi \eta_{soot})^{1/3} \left( \frac{6M_{soot}}{\rho_{soot}} \right)^{2/3} \quad (14)$$

At the right hand side of the equation, the first and second terms represent the rate of increase in soot mass by particle inception and surface growth respectively, while the third term denotes the rate of decrease in soot mass by oxidation of particles. In the particle inception rate term,  $W_{soot}$  is the average molecular weight of the

soot incipient given as 144 kg mol<sup>-1</sup>,  $Z_{C_2H_2}$  is the mole fraction of acetylene,  $R_{gas}$  is the universal gas constant,  $\tilde{P}$  and  $\tilde{T}$  are the field pressure and temperature for the fluid mixture,  $C$  and  $E$  are the pre-exponential constant and activation energy respectively, with subscripts  $\alpha$ ,  $\gamma$  and  $\omega$ . In the surface growth rate term,  $\eta_{soot}$  is the number density for soot particles and the average density of soot particle  $\rho_{soot}$  is taken as 1800 kg m<sup>-3</sup>. In the soot oxidation term, the collisional efficiency  $C_{coll}$  is given as 0.04 and  $Z_{OH}$  is the mole fraction of hydroxide. For the number density, the source term is provided as follows:

$$S_{\eta_{soot}} = C_\alpha N_A \left( \frac{Z_{C_2H_2} \tilde{P}}{R_{gas} \tilde{T}} \right) \exp \left( -\frac{E_\alpha}{\tilde{T}} \right) - C_\beta \left( \frac{24 R_{gas} \tilde{T}}{\rho_{soot} N_A} \right)^{1/2} D_{soot}^{1/2} \eta_{soot}^2 \quad (15)$$

where the first and second terms at the right indicate the change in number density by particle inception and coagulation rates in which the subscript  $\beta$  represents coagulation rate,  $N_A$  is the Avogadro number (i.e.  $6.0221 \times 10^{26}$  k mol<sup>-1</sup>) and  $D_{soot}$  is the mean diameter of soot particles. The activation energies for empirical rates of particle inception, surface growth, coagulation and surface growth can be found in the soot formation kinetics study performed by Leung et al. [51], whereas the values for pre-exponential constants are provided through numerical simulation parametric study [52].

## 2.8. Radiation heat exchange modelling

In this study, the radiative heat transfer is modelled using the filtered radiative transfer equations (FRTE) for non-scattering grey gas solved by the discrete ordinates method (DOM) with the S<sub>4</sub> quadrature scheme accordingly to Jamaluddin and Smith [53]. The S<sub>4</sub> numerical quadrature with the maximum number of 24 discrete ordinates is applied for the integrals over the solid angles. The discrete radiation source term  $\bar{S}_{rad}$  that appears in the energy equation is determined as:

$$\bar{S}_{rad} \approx -4\bar{k}_a E_b + \sum_{j=1}^{24} w_j \bar{k}_a \bar{I}_j \quad (16)$$

where the blackbody radiation is represented by  $E_b = \sigma T^4$ ,  $\sigma$  is the Stefan-Boltzmann constant and  $T$  is the temperature.  $\bar{I}_j$  is the radiation intensities that span over the solid angles range of  $4\pi$  around a point in space. The Weighted Sum of Grey Gases Model (WSGGM) according to Beer et al. [54] was used to approximate the filtered gas absorption coefficient  $\bar{k}_a$  for each combustion products as well as the unburned fuel. This method considers a one-clear two-gray gases representation similar to the consideration proposed by Truelove [55]. The overall absorption coefficient can be expressed as a summation of the coefficients of all the species of the gas mixture and soot:

$$\bar{k}_a = \bar{k}_{a,g} + \bar{k}_s \quad (17)$$

where  $\bar{k}_{a,g}$  and  $\bar{k}_s$  are the absorption coefficients for the gas mixture and soot respectively. The gas mixture coefficient is given by:

$$\bar{k}_{a,g} = \sum_{i=1}^i a_{e,i} \alpha_i P \quad (18)$$

where  $a_{e,i}$  is the emissivity weight-factor for the  $i$ -th grey gas,  $\alpha_i$  is the absorption coefficient for the  $i$ -th grey gas and  $P$  is the sum of the partial pressures of the gases. The absorption coefficient for

soot particles is determined in terms of the volume fraction and temperature according to Kent and Honnery [56]:

$$\bar{k}_s = 1862 f_v T \quad (19)$$

where  $f_v$  is the soot volume fraction.

## 2.9. Numerical procedure

The fire code utilised in this study is written in FORTRAN programming language and the logical flow of the code is illustrated in Fig. 4. The fire code can be divided into six distinct modules: (i) a gas-phase laminar module, (ii) a turbulence module using the LES framework, (iii) a combustion module, (iv) a radiation module, (v) a soot formation module and (vi) level set module for fire spread. The methodology, based on an implicit procedure for the pressure-velocity linkage, is solved iteratively via matrix solvers which has been reported in previous works [57]. The simulations were performed on an Intel Core i5-6400T 2.2 GHz PC with 4GB RAM. For each iteration time step, the code executes the following procedures to account for the complex turbulent reacting flow of the fire spread over the pine-needle board:

*Step 1:* Update thermodynamic properties, calculate diffusion and convection terms for velocity and other field variables and upload boundary conditions

*Step 2:* Apply pressure-velocity linkage method to update pressure field.

*Step 3:* Calculate spread rate and solve for level-set equations to determine the flame front. The burnt cells are prescribed with a gas-phase fuel injection.

*Step 4:* Implement subgrid-scale (SGS) turbulence model to evaluate turbulent viscosity and apply boundary treatment for turbulence equations.

*Step 5:* Update mixture fraction, eddy viscosity and solve heat release rate through combustion as well as evaluating the mass fraction of considering chemical species.

*Step 6:* Calculate radiation heat exchange between gaseous products (i.e. CO, CO<sub>2</sub> and soot particles) and compartment closures.

*Step 7:* Solve energy equation based on the updated combustion and radiation source terms.

*Step 8:* Evaluate soot particle field with the computational domain.

*Step 9:* Advance the solution in time.

## 3. Case study of fire spread over a pine needle board

### 3.1. Experimental arrangements

The experimental work considered in this study is a series of fire test carried out by Liu et al. [36] to investigate the effect of slope on the spread of a linear flame front. The experiment was conducted on a 6 m × 1.8 m working bench within a 9.4 m × 9.4 m × 16 m enclosed test hall facility. The bench was installed onto a motor driven steel frame that is inclinable for slope angles up to 30°. A one meter wide pine needle board was inserted to the bench along with two 10 cm tall metal sheets on each side. The sheets were installed to recreate a uniform linear flame front by suppressing the entrainment from both sides of the fuel bed. The setup of the experiment is shown in Fig. 5. The pine needle board was ignited at the edge with a small amount of *n*-heptane fuel.

Gas temperatures along the fuel bed were measured using 26 thermocouples positioned 2 cm over the fuel bed and approximately 20 cm apart. The exact positions were marked on Fig. 5(a). As mentioned previously, the fuel used in the experiment is dead pine needles (*Pinus sylvestris*) from north-east China. Material properties for *Pinus sylvestris* were reported by Liu et al. [36] and it should

**Table 5**  
Material property of Pine Needle.

Fuel	Dead pine needle ( <i>Pinus sylvestris</i> )
Density	583 kg m <sup>-3</sup>
Surface area to volume	4710 m <sup>-1</sup>
Heat value	21000 kJ kg <sup>-1</sup>
depth	0.04 m
Total fuel load	0.7 kg m <sup>-2</sup>

**Table 6**

Moisture contents and length of pine needle board for corresponding cases with different slope angles.

Case Number	Slope Angle (°)	Moisture Content (%)	Length of pine needle board (m)
1	0	8.7	3.8
2	5	9.2	3.8
3	10	9.8	3.8
4	15	9.9	3.8
5	20	8.4	3.8

be noted that the pine needle board is homogenous, meaning that the material property applied throughout the board is consistent, which are summarised in Table 5.

For the purpose of minimising computational time duration, five cases with 3.8 m long pine needle boards were selected in this numerical study. It should be noted that different moisture contents were measured during each experimental test. The recorded conditions are used as inputs for the initial pine needle board wetness conditions in all the simulation cases. Further details including the slope angles and initial settings applied for each simulation cases can be referred to Table 6.

### 3.2. Modelling configuration and boundary conditions

The three-dimensional computational domain of the pine needle board (in blue) sealed within the working bench (in metallic grey) is depicted in Fig. 6(a). It is designed as a rectangular box with a size of 1.8 m × 4.8 m × 5 m. The length of the working bench is 3.8 m long and both ends in the x-direction are extended by 0.5 m to allow incoming/outgoing flow to be fully modelled before it approaches the fuel bed region. Besides the flooring (lower XY plane), all five outer surfaces are prescribed as opening boundary conditions. As shown in Fig. 6(b), a series of blockages with 0.1 m length is used to represent the 1 m × 3.8 m fuel bed, in which each blockage surface is associated with a level-set term value reflecting the position of the fire. The simulation is initialised by assigning a -1 value to the first row of block surface to represent the ignition of the pine needle board by *n*-heptane. At each time instance, the fire spread model maps out the flame front and the corresponding surfaces with negative level-set terms will activate the gas-phase combustion model.

### 3.3. Mesh sensitivity analysis

Four uniform mesh systems were numerically studied to examine the mesh independence of this case study. The characteristic length scale (DiNenno et al. [58]) was used to determine the mesh sizes, the details are summarised in Table 7. Mesh sensitivity analysis was performed to determine the appropriate mesh system for this simulation. For the purpose of reducing the computational time required for the test, the results for thermocouple T3 was compared for different meshes since it is closest to the ignition point (i.e. position 1.14 m along the pine needle fuel bed). As illustrated in Fig. 7, the temperature converged significantly from the coarse 0.1 m mesh to the 0.075 m mesh. There is a smaller difference upon further refinement from the 0.075 m to the 0.05 m. Further

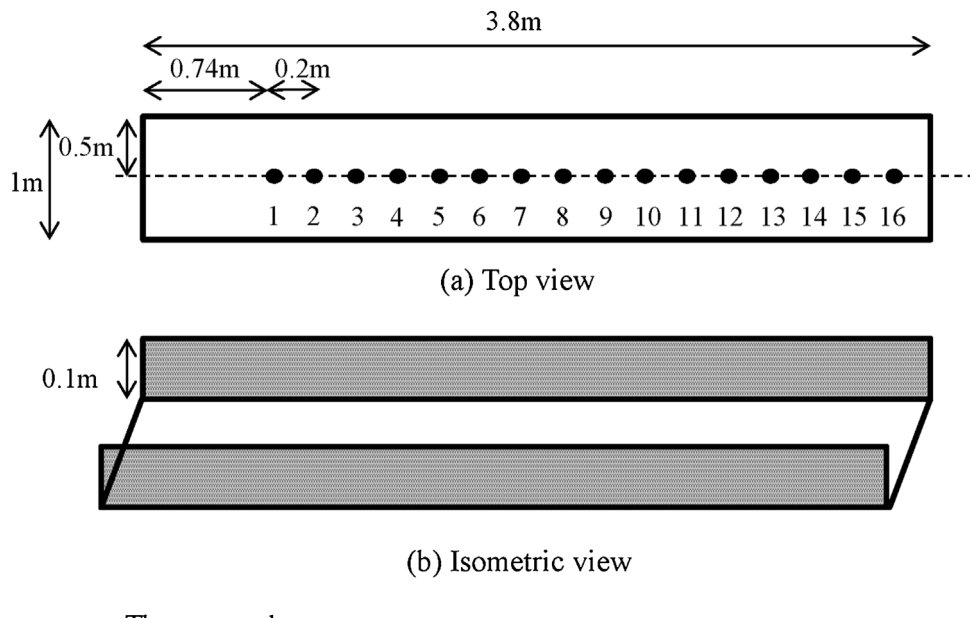


**Fig. 5.** Experimental configurations showing the dimensions of the fuel bed and location of the thermocouples. (a)Top view (b) Isometric view.

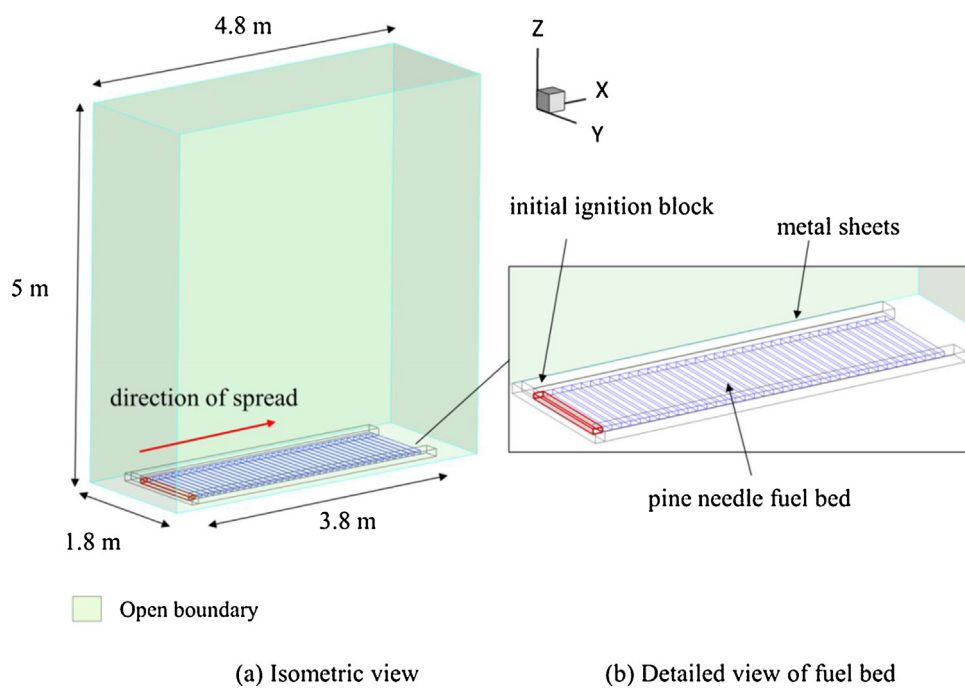


**Fig. 6.** Dimensions of the computational domain adopted during the simulation. (a) Isometric view (b) Detailed view of the fuel bed.

**Table 7**  
Summary of the mesh systems used in the mesh sensitivity analysis.

Mesh number	Mesh size (m)	Total number of cells	$R^*$ range
1	0.1	43200	$1/15 < R^* < 1/5$
2	0.075	102400	$1/15 < R^* < 1/10$
3	0.05	345600	$1/15 < R^* < 1/10$
4	0.04	675000	$1/15 < R^* < 1/10$

mesh refinement from 0.05 m makes minor differences in the peak temperature. The peak temperatures converged by approximately 33.4% from the coarse 0.1 m mesh to the 0.075 m mesh and approximately 2.5% from the 0.075 m to the 0.05 m mesh. Taking into

consideration the convergence results, the 0.05 m uniform mesh was adopted in this numerical simulation. The same mesh configuration is shared between the fire spread model and the gas-phase combustion model. The computational time for the simulations with 345,600 mesh cells are approximately 10s/hr (i.e. it takes 1 h to simulate 10 s in the model.) The longest duration occurs in the no slope ( $0^\circ$ ) case with a burn time of approximately 1500s.

#### 4. Results and discussions

Numerical results from all five cases are presented in this section. The simulations are distinguished by the slope angle (ranging

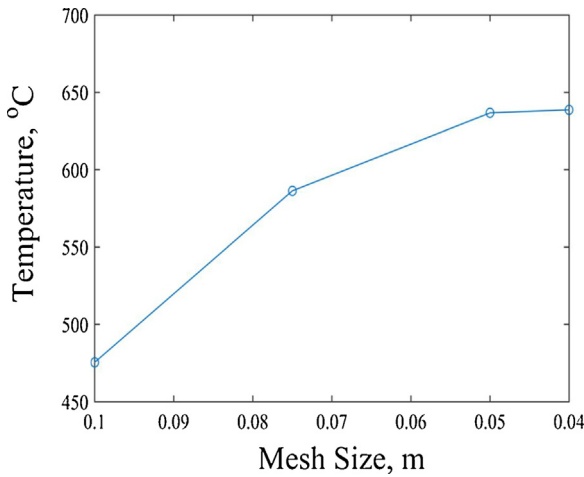


**Fig. 7.** Peak gas temperature predictions at thermocouple (T3) for mesh size: 0.1 m, 0.075 m, 0.05 m and 0.04 m.

from 0 °C to 20 °C) and the corresponding moisture content of the pine needle.

#### 4.1. Temperature predictions versus thermocouple measurements

The numerical results were compared to the experimental measurements provided by Liu et al. [59]. It should be addressed that a 5 s moving time average was adopted on the numerical results to remove small fluctuations of temperature generated by the model and illustrate a more stable data over time. The smoothing algorithm provides an improved visualisation of the simulation results and better comparison with the experiments. Fig. 8 illustrates the comparison between raw simulation and time-averaged data. Some of the thermocouples were not plotted to avoid overloading the figures. The sudden temperature spikes at the thermocouples represent the arrival time of the flame front and the fluctuating smaller peaks following the initial spike represent the burn time and the decrease in temperature indicate that the fuel was burnt out.

Figs. 9 and 10 indicate temperature predictions at various thermocouple locations along the fuel bed for inclined slope angles of 5° and 20° respectively. The model predictions for both cases are

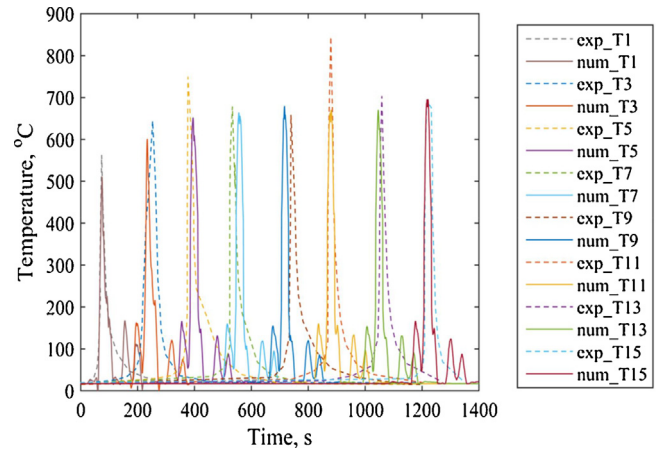


**Fig. 9.** Gas temperature measurements for thermocouples T1–T15 from the experiment (in dotted line) and numerical predictions (in solid line) for slope angle 5°.

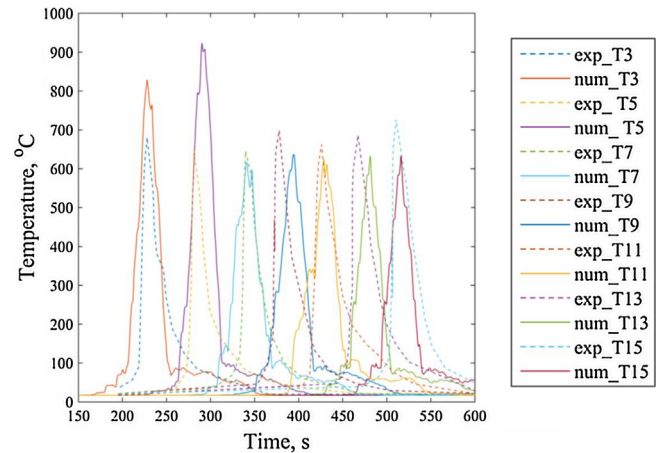


**Fig. 10.** Gas temperature measurements for thermocouples T3–T15 from the experiment (in dotted line) and numerical predictions (in solid line) for slope angle 20°.

in reasonable agreement with the experimental measurements of Liu et al. [36]. Occurrence times of the temperature increase were captured by the simulation. This suggests that the flame front posi-

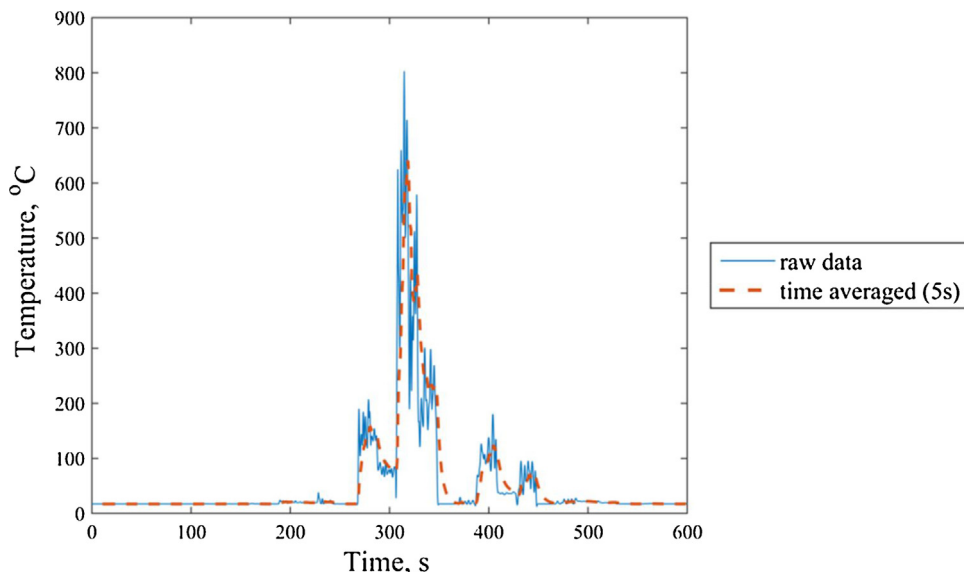


**Fig. 8.** Comparison of gas temperature predictions at thermocouple (T3) between raw and time averaged simulation data.

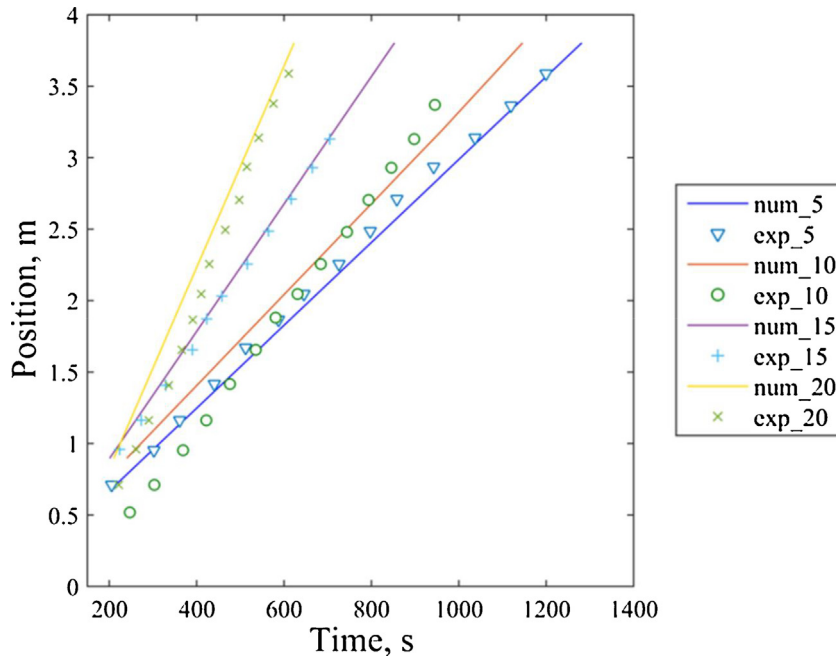


**Fig. 11.** Comparisons of predicted and experimental flame front position over time for slope angles 5°, 10°, 15° and 20°.

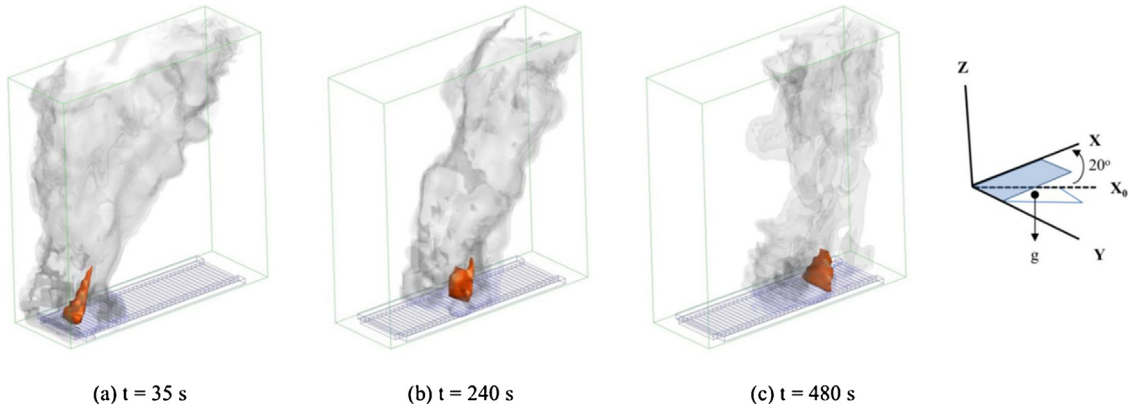


**Fig. 12.** 3D isometric surface plot illustrating flame movement and smoke generation at different time for slope angle 20° simulation.

tion is aptly predicted. The slope angle 20° results showed more build up before the initial temperature spike and retain a higher residual temperature after the flame has passed for each thermocouple when compared to the 5° case. The peak temperature is also higher for steeper inclines, the average peak temperature for the 5° and 20° case are approximately 603°C and 696°C respectively. Numerical peak thermocouple temperatures and the interval of each burning period are also in fair concurrence with the experiment. The average error for the peak temperature between model prediction and measured data was approximately 11.07%.

The errors in the prediction can be attributed to a few factors: (i) The accuracy of the fire spread rate using Rothermel's [4] model and the input variables used in the formulation, (ii) the fire propagation assumes a constant spread rate, therefore the interval between each temperature spike will be the same. On the other hand, the experimental results were non-uniform, there are slight discrepancies in the rate of spread at the intervals between thermocouple positions.

#### 4.2. Fire spread rate comparisons

The flame front position over time measured in the experiment and numerical modelling for slope angles between 5 and 20 are

displayed in Fig. 11. In this study, the comparison is between the periods where the spread rate has stabilised as data for the initial acceleration phase of the fire spread was removed in the experimental measurements and the model assumes a constant spread rate through the whole simulation. The flame front position was obtained directly from the level-set based fire spread model.

As can be seen in Fig. 11, the simulation predicted results are in relatively good agreements with the experimental measurements. With increasing slope angle, the rate of fire spread also increased. The burning duration of the slope angle 5° case was approximately 1400 s while the slope angle 20° reduced significantly to approximately 502 s. It should be noted that the numerical fire spread rate can be calculated as the slope of the flame front position lines. Accordingly, the calculated rates of spread for the simulation cases were compared with the experimental data and summarised in Table 8. The average error between the predictions and experimental measurements is approximately 3%. Note that there was a significantly higher spread rate of  $0.0038 \text{ m s}^{-1}$  measured for the 10° slope case. In the original experiment, Liu et al. [36] conducted three 10° cases under similar conditions and the other two cases both recorded a spread rate of  $0.0029 \text{ ms}^{-1}$ . This anomaly for the 10° slope case could be due to factors that were not considered in

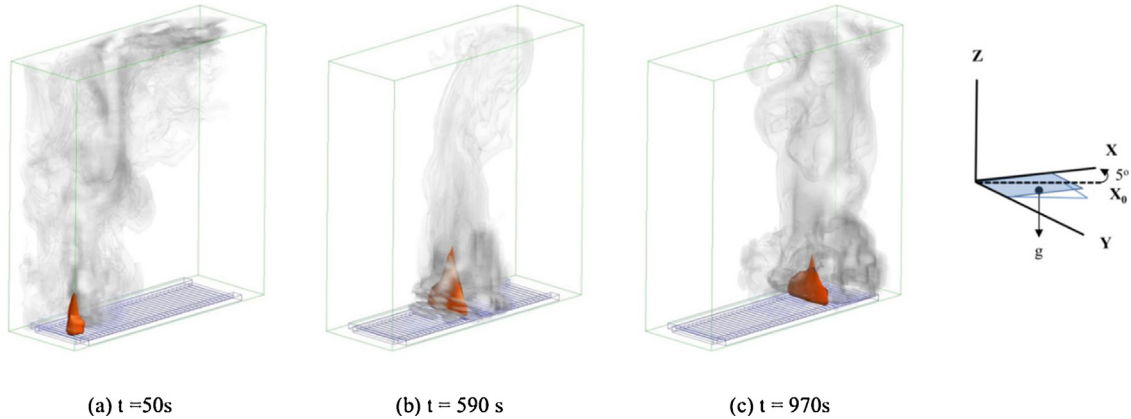


**Fig. 13.** 3D isometric surface plot illustrating flame movement and smoke generation at different time for slope angle 5° simulation.

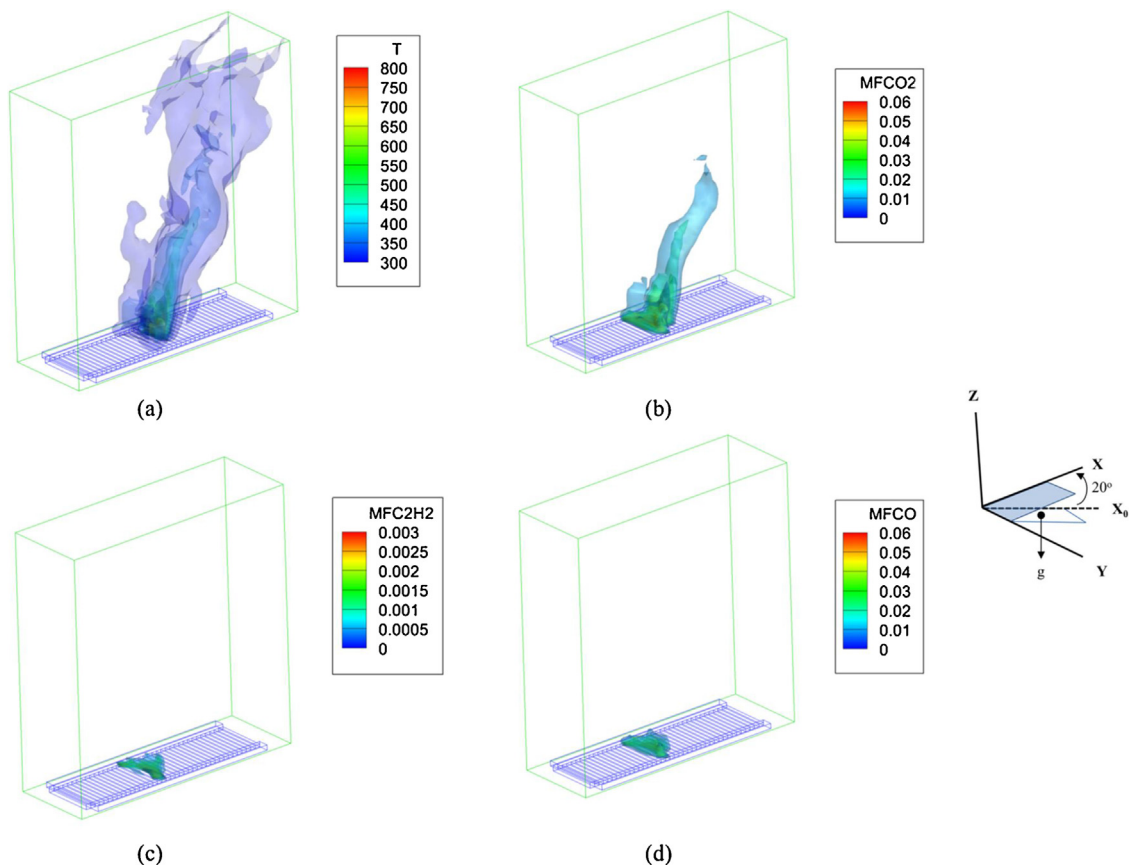


**Fig. 14.** 3D isometric contour plot for (a) temperature and intermediate species: (b) CO<sub>2</sub>, (c) C<sub>2</sub>H<sub>2</sub>, (d) CO for slope angle 20° simulation at t = 240s.

**Table 8**

Experimental and Model rate of fire spread results, calculated using linear regression.

Case Number	Slope Angle ( $^{\circ}$ )	Experimental ROS (ms $^{-1}$ )	Model ROS (ms $^{-1}$ )
1	0	0.0027	0.00260
2	5	0.0029	0.00290
3	10	0.0038	0.00314
4	15	0.0045	0.00446
5	20	0.0074	0.00704

the experiment such as wind or ambient conditions. In comparison to the flat plane fire spread (cases 1–2), the deviation from the experiment is slightly larger for the 20° slope case (case 5) which is around 4.8%. In general, it is demonstrated that the slope effect

is reasonably captured in the adopted fire spread model hence the fire code is able to replicate the flame front location.

#### 4.3. Flame region and smoke layer visualisation

By applying three-dimensional LES modelling approach, the full duration of the fire spread can be visualised by the three-dimensional isometric view plots. Figs. 12 and 13 show the three-dimensional isometric plot for the flame movement and its corresponding smoke generation visualised by a gas temperature cut off at  $490^{\circ}\text{C}$  (in red) and soot volume fraction of 0.1 (in grey) respectively over time. It should be noted that the slope angle is applied in the model by tilting the horizontal plane (i.e. adjusting the gravitational forces). As demonstrated in Fig. 11, the titled hori-

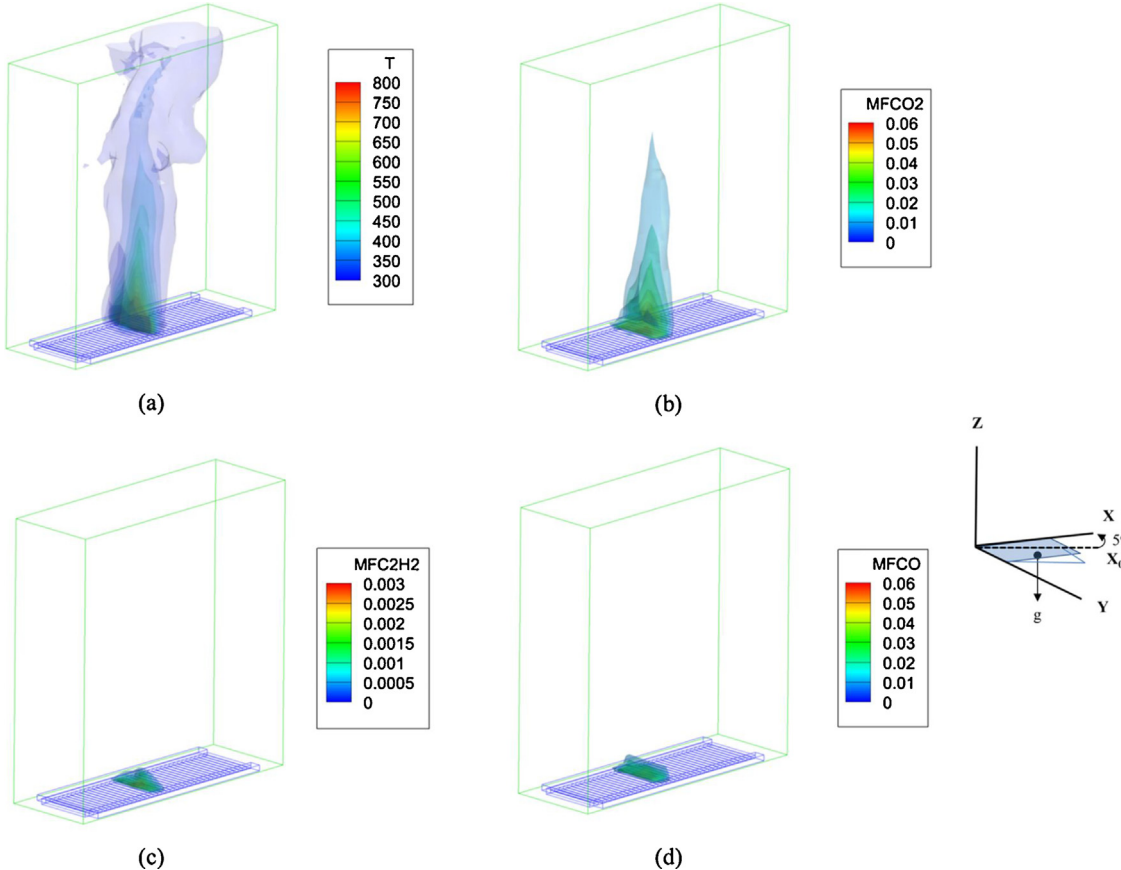


**Fig. 15.** 3D isometric contour plot for (a) temperature and intermediate species: (b)  $\text{CO}_2$ , (c)  $\text{C}_2\text{H}_2$ , (d) CO for slope angle  $5^\circ$  simulation at  $t = 590\text{s}$ .

horizontal plane (XY-plane) is ascended by a slope angle of  $20^\circ$  relative to the original plane ( $X_0Y$ -plane), in which the gravitational vector  $\mathbf{g}$  is perpendicular to the original horizontal plane. The plots (a), (b) and (c) correspond to the time instance when the flame front is at positions: 0.2 m, 1.7 m and 2.8 m for slope angle:  $20^\circ\text{C}$  and  $5^\circ\text{C}$  case respectively. The smoke generation is modelled by the Moss-Brookes semi-empirical soot model. Since this model applies “acetylene” ( $\text{C}_2\text{H}_2$ ) as the main soot precursor, it can be seen that most of the soot are concentrated at the flame core region where the amount of  $\text{C}_2\text{H}_2$  is the richest. Utilising soot volume fraction as an indicator for smoke, the model is able to capture the evolution of the buoyancy driven smoke plumes

The results showed that steeper slope angle increases the rate of fire spread as observed in both experimental studies reported by Liu [36] and Dupuy [60]. Due to buoyancy, flame tends to ascend vertically upwards. Hence, for the sloped cases, the flame will be tilted. The flame tilts increasingly towards the fuel bed as the slope angle increases. This effect is further amplified by the unbalance of entrainment conditions that create a larger upslope flow, pushing the flame towards the spreading direction. This phenomenon raises the radiation heat transfer from the flame to the fuel bed and encourages faster flame spread.

#### 4.4. Major and intermediate combustion products

Through the consideration of detailed chemistry for  $\text{CH}_2\text{O}$ , the complete description of the formation processes for the intermediate chemical species are enabled. This allows the fire code to provide a reliable prediction of key asphyxiant gases such as  $\text{CO}/\text{CO}_2$ , as well as the well-recognised soot precursor  $\text{C}_2\text{H}_2$  [32]. Three-dimensional isometric contour plots for the concentration

of  $\text{CO}_2$ ,  $\text{CO}$  and  $\text{C}_2\text{H}_2$  are displayed in Figs. 14 and 15(a), (b) & (c) respectively. In addition, the temperature profile is shown in Figs. 14 and 15(d) to provide a visualisation of the flame and the flow of the hot plume gas corresponding to the species contour plots. The majority of the CO forms at near the flame core region, while  $\text{CO}_2$  can reach to a height level of around 5 m. This is due to the fact that most CO will be converted to  $\text{CO}_2$  when it is oxidised by the surrounding air. As depicted in Fig. 14(c), (d), the mass fraction of  $\text{C}_2\text{H}_2$  and CO is not significant since the size of the fire is small (around 60 kW) and this case is very well ventilated with most of the computational domain covered with oxygen.

## 5. Conclusions

A three-dimensional in-house fire code incorporating SGS turbulence, combustion, soot formation and radiation sub-modelling components for the gas phase has been developed specifically for bush and forest fire modelling. A level-set methodology to track the flame front is incorporated to determine the burning region. The proposed fire code that uniquely embraces the detailed chemical kinetics fully describes the gas-phase combustion process of the fire and the prediction of the smoke layer.

In order to validate the proposed fire code and examine its effectiveness in fire spread scenarios, numerical simulations were performed on a series of fire spread experiments on pine needle board under different slope conditions. The numerical predictions were found to agree very well with the experimental data in terms of the rate of fire spread and temperature. Occurrence times of temperature peaks caused by the flame front recorded at each thermocouple location were adequately captured by the numerical simulation. Peak thermocouple temperatures and the interval

of each burning period have been found to be in good agreement with experiment. The linking of the fire spread model with the gas-phase model allows not only for gas-phase fluid interactions but also predictions of the concentrations of the combustion products and smoke particles. Essentially, the code was able to provide the concentrations of toxic volatiles such CO and CO<sub>2</sub> and the smoke layer formation via the Moss-Brookes semi-empirical soot model. All the prediction data that was rendered into three dimensional isometric figures depicted instantaneous mass fractions of emissions released by the fire and distributed by the hot plume flow.

Based on the key findings addressed in this article, the following future works are suggested: Firstly, small-scale pine needle board experiments should be performed with detailed gas volatile and soot particle measurements. Secondly, the fire code developed in this study fully resolves the heat transfer mechanisms (e.g. radiation) for a linear flame front under a slope condition. The slope effect is currently considered by an empirical model, therefore the development of a two-way feedback between the level-set fire spread model and the LES model may improve the spread rate predictions under different slope angles. Thirdly, numerical simulation should be performed on larger case studies including full-scale grass or forest fires to validate the fire code against more realistic fire scenarios. Lastly, another approach to consider the slope effect may be to develop and apply a solid pyrolysis model and coupled with the radiation model to account for the complex interactive phenomena of radiation heat feedback from the fire source towards the solid fuel. All the above points will be investigated in our future works.

In summary, a LES fire code has been developed to include the following advancing features:

- (i) the incorporation of detailed chemical kinetics to consider the full description of the oxidation process of the fuel, as well as the formation mechanisms for intermediate products such as CO and C<sub>2</sub>H<sub>2</sub>;
- (ii) the gas-phase temperature field at the flaming region is reasonably predicted in comparison with experimental measurements by the fire spread and combustion models;
- (iii) the smoke layer generated at the flame front is modelled based on a semi-empirical soot formation model with all essential soot generation and reduction kinetics such as particle inception, surface growth, coagulation and oxidation where acetylene is considered as the soot precursor;
- (iv) by enabling the predictions for soot particles and other gaseous combustion products, the radiation heat exchange at the flame front and its corresponding hot fire plume is aptly simulated.

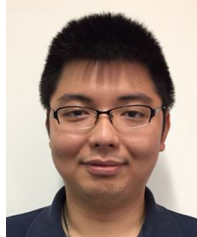
## Funding

The paper is supported by the Australian Research Council (ARC Linkage Project LP140100121). All financial and technical supports are deeply appreciated by the authors.

## References

- [1] B. Teague, R. McLeod, S. Pascoe, Victorian Bushfires Royal Commission Interim Report, Parliament of Victoria, Melbourne, 2009.
- [2] M.G. Cruz, A.L. Sullivan, R. Leonard, S. Malkin, S. Matthews, J.S. Gould, W.L. McCaw, M.E. Alexander, Fire Behaviour Knowledge in Australia Spread Prediction Capability and Application, 2014.
- [3] A.L. Sullivan, Wildland surface fire spread modelling, 1990–2007. 2: empirical and quasi-empirical models, *Int. J. Wildland Fire* 18 (2009) 369–386.
- [4] R.C. Rothermel, A mathematical model for predicting fire spread in wildland fuels, in: USDA Forest Service Research Paper INT USA, 1972, pp. 40.
- [5] J.H. Scott, R.E. Burgan, Standard Fire Behavior Fuel Models: A Comprehensive Set for Use with Rothermel's Surface Fire Spread Model, 2005, pp. 72.
- [6] L.S. Bradshaw, J.E. Deeming, R.E. Burgan, J.D. Cohen, The national fire-danger rating system—1978, in: USDA Forest Service General Technical Report INT-169, 1983, pp. 1–49.
- [7] P. Andrews, BehavePlus fire modeling system: past, present, and future, *Proceedings of 7th Symposium on Fire and Forest Meteorological Society* (2007) 13.
- [8] R.C. Rothermel, H.E. Anderson, Fire spread characteristics determined in the laboratory, in: USDA Forest Serv. Intermountain Forest Range Exp. Station Res. Paper INT-30, 1966, 34 p.
- [9] A.G. McArthur, Weather and Grassland Fire Behaviour, Forestry and Timber Bureau, Canberra, 1966.
- [10] A.L. Sullivan, Wildland surface fire spread modelling, 1990–2007. 1: physical and quasi-physical models, *Int. J. Wildland Fire* 18 (2009) 349.
- [11] J.H. Balbi, F. Morandini, X. Silvani, J.B. Filippi, F. Rinieri, A physical model for wildland fires, *Combust. Flame* 156 (2009) 2217–2230.
- [12] Forestry Canada Fire Danger Group, Development and Structure of the Canadian Forest Fire Behavior Prediction System. Information Report ST-X-3, 1992, in, Ottawa, Ontario.
- [13] G. Bianchini, P. Caymès-Scutari, M. Méndez-Garabetti, Evolutionary-statistical system: a parallel method for improving forest fire spread prediction, *J. Comput. Sci.* 6 (2015) 58–66.
- [14] G. Sanjuan, C. Brun, T. Margalef, A. Cortés, Determining map partitioning to minimize wind field uncertainty in forest fire propagation prediction, *J. Comput. Sci.* 14 (2016) 28–37.
- [15] M.A. Finney, FARSITE. Fire Area Simulator-model Development and Evaluation. Res. Pap. RMRS-RP-4, Revised 2004, U.S. Department of Agriculture, Forest Service, Rocky Mountain Research Station, Ogden, UT, 1998, 47 p.
- [16] K. Tolhurst, D. Chong, M. Strandgard, Wildfire risk management model for strategic management, *For. Ecol. Manage.* (2006).
- [17] M. Rochoux, C. Emery, S. Ricci, B. Cuenot, A. Trouvé, Towards predictive data-driven simulations of wildfire spread—part II: Ensemble Kalman filter for the state estimation of a front-tracking simulator of wildfire spread, *Nat. Hazards Earth Syst. Sci.* 15 (2015) 1721–1739.
- [18] J.B. Filippi, F. Bosseur, C. Mari, C. Lac, P. Le Moigne, B. Cuenot, D. Veynante, D. Cariolle, J.H. Balbi, Coupled atmosphere-wildland fire modelling, *J. Adv. Model. Earth Syst.* 1 (2009).
- [19] R. Linn, F. Harlow, FIRETEC: A Transport Description of Wildfire Behavior, 1997, pp. 836.
- [20] W.E. Mell, S.L. Manzello, A. Maranghides, Numerical modeling of fire spread through trees and shrubs, *For. Ecol. Manage.* 234 (2006) S82.
- [21] G.A. Trunfio, D.D. Ambrosio, R. Rongo, W. Spataro, S.D. Gregorio, A new algorithm for simulating wildfire spread through cellular automata, *ACM Trans. Model. Comput. Simul.* 22 (2011) 1–26.
- [22] J.A. Sethian, Level Set Methods and Fast Marching Methods, Cambridge University Press, 1999, pp. 1–33.
- [23] R.G. Rehm, R. McDermott, Fire-Front Propagation Using the Level Set Method, 2009, pp. 1–12.
- [24] J. Mandel, J.D. Beezley, A.K. Kochanski, Coupled atmosphere-wildland fire modeling with WRF 3.3 and SFIRE 2011, *Geosci. Model Dev.* 4 (2011) 591–610.
- [25] J. Reisner, J. Bossert, J. Winterkamp, Numerical Simulation of Two Wildfire Events Using a Combined Modeling System, BEHAVE, HIGRAD, 1998.
- [26] J. Reisner, S. Wynne, L. Margolin, R. Linn, Coupled Atmospheric–Fire Modeling Employing the Method of Averages, 2000.
- [27] A.C.Y. Yuen, G.H. Yeoh, B. Alexander, M. Cook, Fire scene investigation of an arson fire incident using computational fluid dynamics based fire simulation Building Simulation, vol. 7, Springer, 2014, pp. pp. 477–487.
- [28] D. Morvan, J.L. Dupuy, Modeling the propagation of a wildfire through a Mediterranean shrub using a multiphase formulation, *Combust. Flame* 138 (2004) 199–210.
- [29] W. Mell, M.A. Jenkins, J. Gould, P. Cheney, A physics-based approach to modelling grassland fires, *Int. J. Wildland Fire* 16 (2007) 1.
- [30] A.C.Y. Yuen, G.H. Yeoh, V. Timchenko, S.C.P. Cheung, T. Chen, Study of three LES subgrid-scale turbulence models for predictions of heat and mass transfer in large-scale compartment fires, *Numer. Heat Transfer, Part A Appl.* 69 (2016) 1223–1241.
- [31] N.P. Cheney, J.S. Gould, W.R. Catchpole, Prediction of fire spread in grasslands, *Int. J. Wildland Fire* 8 (1998) 1.
- [32] A.C.Y. Yuen, G.H. Yeoh, V. Timchenko, S.C.P. Cheung, T.J. Barber, Importance of detailed chemical kinetics on combustion and soot modelling of ventilated and under-ventilated fires in compartment, *Int. J. Heat Mass Transfer* 96 (2016) 171–188.
- [33] J.L. Dupuy, J. Maréchal, Slope effect on laboratory fire spread: contribution of radiation and convection to fuel bed preheating, *Int. J. Wildland Fire* 20 (2011) 289.
- [34] J.L. Dupuy, M. Larini, Fire spread through a porous forest fuel bed: a radiative and convective model including fire-induced flow effects, *Int. J. Wildland Fire* 9 (1999) 155–172.
- [35] F. Morandini, P.A. Santoni, J.H. Balbi, The contribution of radiant heat transfer to laboratory-scale fire spread under the influences of wind and slope, *Fire Saf. J.* 36 (2001) 519–543.
- [36] N. Liu, J. Wu, H. Chen, X. Xie, L. Zhang, B. Yao, J. Zhu, Y. Shan, Effect of slope on spread of a linear flame front over a pine needle fuel bed: experiments and modelling, *Int. J. Wildland Fire* 23 (2014) 1087.
- [37] J.A. Sethian, Evolution, implementation, and application of level set and fast marching methods for advancing fronts, *J. Comput. Phys.* 169 (2001) 503–555.
- [38] S. Osher, R. Fedkiw, Level Set Methods and Dynamic Implicit Surfaces, 1 ed., Springer-Verlag, New York, 2003.

- [39] F.X. Jervis, G. Rein, Experimental study on the burning behaviour of *Pinus halepensis* needles using small-scale fire calorimetry of live, aged and dead samples, *Fire Mater.* 40 (2016) 385–395.
- [40] C. Jiménez, F. Ducros, B. Cuenot, B. Beïdat, Subgrid scale variance and dissipation of a scalar field in large eddy simulations, *Phys. Fluids* 13 (2001) 1748.
- [41] A. Yoshizawa, K. Horiuti, A statistically-derived subgrid-scale kinetic energy model for the large-eddy simulation of turbulent flows, *J. Phys. Soc. Jpn.* 54 (1985) 2834–2839.
- [42] R.W. Bilger, Reaction rates in diffusion flames, *Combust. Flame* 30 (1977) 277–284.
- [43] R.K.K. Yuen, G.H. Yeoh, G.D. Davis, E. Leonardi, Modelling the pyrolysis of wet wood—I. Three-dimensional formulation and analysis, *Int. J. Heat Mass Transfer* 50 (2007) 4371–4386.
- [44] D. Drysdale, An Introduction to Fire Dynamics, John Wiley & Sons, New York, 1985.
- [45] G.P. Smith, D.M. Golden, M. Frenklach, N.W. Moriarty, B. Eiteneer, M. Goldenberg, C.T. Bowman, R.K. Hanson, S. Song, W.C. Gardiner Jr., V.V. Lissianski, Z. Qin, GRI-Mech 3.0, 2000.
- [46] R.J. Kee, F.M. Rupley, J.A. Miller, M.E. Coltrin, J.F. Grcar, E. Meeks, CHEMKIN Collection, Release 3.6, Reaction Design, Inc., San Diego, CA, US, 2000.
- [47] Computational Fluid Dynamics in Fire Engineering, in: G.H. Yeoh, K.K. Yuen (Eds.), 1st edition, Butterworth-Heinemann, Burlington, 2009.
- [48] S.C.P. Cheung, G.H. Yeoh, A. Cheung, R.K.K. Yuen, S.M. Lo, Flickering behavior of turbulent buoyant fires using large-eddy simulation, *Numer. Heat Transfer, Part A Appl.* 52 (2007) 679–712.
- [49] G. Erlebacher, M.Y. Hussaini, C.G. Speziale, T.A. Zang, Toward the large-eddy simulation of compressible turbulent flows, *J. Fluid Mech.* 238 (1992).
- [50] S.B. Dworkin, Q. Zhang, M.J. Thomson, N.A. Slavinskaya, U. Riedel, Application of an enhanced PAH growth model to soot formation in a laminar coflow ethylene/air diffusion flame, *Combust. Flame* 158 (2011) 1682–1695.
- [51] K.M. Leung, R.P. Lindstedt, W.P. Jones, A simplified reaction mechanism for soot formation in nonpremixed flames, *Combust. Flame* 87 (1991) 289–305.
- [52] S.J. Brookes, J.B. Moss, Predictions of soot and thermal radiation properties in confined turbulent jet diffusion flames, *Combust. Flame* 116 (1999) 486–503.
- [53] A.S. Jamaluddin, P.J. Smith, Predicting radiative transfer in rectangular enclosures using the discrete ordinates method, *Combust. Sci. Technol.* 59 (1988) 321–340.
- [54] J.M. Beer, P.J. Foster, R.G. Siddall, Calculation Methods of Radiation Heat Transfer, HFTS Design Report No. 22, AEA Technology, 1971, 1971.
- [55] J.S. Truelove, A Mixed Grey Gas Model for Flame Radiation, United Kingdom Atomic Energy Authority Report, Harwell, in: AERE-R-8494, 1976.
- [56] J. Kent, D. Honnery, A soot formation rate map for a laminar ethylene diffusion flame, *Combust. Flame* 79 (1990) 287–298.
- [57] A.C.Y. Yuen, G.H. Yeoh, Numerical simulation of an enclosure fire in a large test hall, *Comput. Therm. Sci.* 5 (2013).
- [58] P.J. DiNenno, D. Drysdale, C.L. Beyler, D.W. Walton, SFPE Handbook of Fire Protection Engineering, 3rd edition, National Fire Protection Association, Quincy, MA, USA, 2002.
- [59] N. Liu, J. Wu, H. Chen, L. Zhang, Z. Deng, K. Satoh, D.X. Viegas, J.R. Raposo, Upslope spread of a linear flame front over a pine needle fuel bed: the role of convection cooling, *Proc. Combust. Inst.* 35 (2015) 2691–2698.
- [60] J.L. Dupuy, J. Maréchal, D. Portier, J.-C. Valette, The effects of slope and fuel bed width on laboratory fire behaviour, *Int. J. Wildland Fire* 20 (2011) 272–288.



**Timothy Bo Yuan Chen** is a Master research student at the School of Mechanical and Manufacturing Engineering at the University of New South Wales. He graduated in 2014 from the same university. His main research interests are computational fluid dynamics (CFD), combustion and wildland fire modelling.



**Anthony Chun Yin Yuen** graduated in December 2014 with a Ph.D. from School of Mechanical and Manufacturing Engineering, University of New South Wales (UNSW), Australia. He is currently continuing as a Research Associate in UNSW. He specialises in building services, computational fluid dynamics (CFD), numerical methods, fluid mechanics and heat transfer, particularly in fire simulations.



**Guan Heng Yeoh** is a Professor from the School of Mechanical and Manufacturing Engineering at the University of New South Wales. He graduated in 1988 and received his Ph.D. in 1993 both from the University of New South Wales. His main fields of interests are computational fluid dynamics (CFD), Numerical Heat and Mass Transfer, Combustion, Radiation Heat Transfer, Soot Formation and Oxidation, Solid Pyrolysis in Fire Modelling, Computational modelling of Magnetic Micro-particles in Mechanical Dampers and Nanofluids with Heat Transfer.



**Victoria Timchenko** is a Senior Lecturer with the School of Mechanical and Manufacturing Engineering at the University of New South Wales. Her research interests include: Computational Fluid Dynamics, Heat Transfer and Hyperthermia and Nanoparticle Transport for biomedical applications (cancer treatment, drug delivery).



**Sherman C.P. Cheung** is an Associate Professor at the School of Mechanical and Automotive Engineering at RMIT University. He received his Ph.D degree in the City University of Hong Kong. His main research interest includes: Computational Fluid Dynamics (CFD), Combustion and Fire Modelling, Computational Modelling of Multiphase Flows and Biomedical Engineering: Simulation of Blood Flow in Arteries.



**Q.N. Chan** is a lecturer at the School of Mechanical and Manufacturing Engineering at the University of New South Wales. He has a B.E. and Ph.D. in engineering from the University of New South Wales. He is an active researcher have strong expertise in developing advanced optical diagnostic tools for the detailed analysis of different practical combustion systems. His main research interest includes: Renewable energy, Combustion, Soot formation and destruction, Laser diagnostics, Alternative fuels and Gas turbines.



**Wei Yang** is a Postdoctor at the State Key Laboratory of Fire Science, University of Science & Technology of China. He has a Joint Ph.D. from the China University of Science and Technology and City University of Hong Kong. His main research interest includes: Nanometer materials, Halogen-free flame retardant, Polymer matrix composites and Flame-retardant mechanism.



**Hongdian Lu** is a Professor from the Department of Chemical and Materials Engineering at Hefei University. He received his Ph.D. from China University of Science and Technology. His main research interest includes: Nanometer materials, flame retardant polymeric nanocomposites and coatings, and flame retardant mechanism.